Time-Domain Performance Bound Analysis of Analog Circuits Considering Process Variations

Xue-Xin Liu*, Sheldon X.-D. Tan*, Zhigang Hao*†, and Guoyong Shi†
*Dept. Electrical Engineering, University of California, Riverside, CA 92521
†School of Microelectronics, Shanghai Jiaotong University, China

***Abstract*—In this paper, we propose a new time-domain performance bound analysis method for analog circuits considering process variations. The proposed method, called *TIDBA*, consists of several steps to compute the bound performances in time domain. First the performance bound in frequency domain is computed for a linearized analog circuits by an variational symbolic analysis method and the Kharitonov's functions. Then the time domain performance bound is computed via a new general-signal transient bound analysis method. The new algorithm can give transient lower bound and upper bound of the performance variations affected analog circuits accurately and reliably. Experimental results from two industry benchmark circuits show that TIDBA gives the correct bounds for the Monte Carlo analysis while it delivers one order of magnitude speedup over the Monte Carlo method.**

I. Introduction

It was well accepted that variations have huge impacts on circuit performance, yield and reliability in the nanometer regime. Analog and mixed-signal circuits in nanometer region are especially sensitive to the process variations as lot of matching and regularities in circuit layout are required. This situation becomes worse as technology continues to scale to 45 nm and below owing to the increasing process-induced variability [9], [14]. For example, due to an inverse-square-root-law dependence with the transistor area, the mismatch of CMOS devices nearly doubles for each process generation less than 90 nm [4], [8]. Since the traditional corner-case based analysis is either too pessimistic or too expensive for practice chip design, the statistical approach thereby becomes imperative to estimate the analog mismatch and performance variations [11]. The variations in the analog components can come from systematic (or global spatial variation) ones and stochastic (or local random variation) ones. In this paper, we model both variations as the parameter intervals on the components of analog circuits.

Monte-Carlo (MC) analysis was applied in the past to analyze the stochastic mismatch and predict the variational responses of their designs under faults. As MC analysis requires a large number of repeated circuit simulations, its computational cost is very expensive. More efficient variational analysis, which can give the performance bounds, is highly desirable.

One viable way of statistical analysis is by means of performance bound or worst case analysis. Bound or worse case analysis of analog circuits has been studied in the past for fault-driven testing and tolerance analysis of analog circuits [5], [17], [19]. The proposed approaches include sensitivity analysis [20], the sampling method [18], and interval arithmetic based approaches [5], [13], [17], [19]. But sensitivity based method can't give the worse case in general and the sampling based method is limited to a few variables. Interval arithmetic methods, in general, have the reputation of overly pessimistic in the past. Recently worst-case analysis of linearized analog circuits in frequency domain has been proposed [13], where Kharitonov's functions [3] were applied to obtain the performance bounds in frequency domain, but no systematic method was proposed to obtain variational transfer functions. In [2], a graph based symbolic and affine interval arithmetic have been applied to compute the variational transfer functions followed by the Kharitonov's functions to obtain the performance bounds in frequency domain. However, no time-domain performance bound analysis of analog circuits based on Kharitonov's functions has been studied and proposed.

In this paper, we propose a new time-domain performance bound analysis method for analog circuits considering parameter variations. The proposed method, called TIDBA (TIme-Domain Bound Analysis), consists of several steps to compute the performance bound in time domain. First the performance bound in frequency domain is computed for a linearized analog circuits by means of determinant decision diagram (DDD)-graph based symbolic analysis, affine arithmetic method and the Kharitonov's functions. After this, the magnitude and phase of the transfer function at each frequency will be obtained. Then the time-domain performance bound is computed via a new general-signal transient bound analysis using FFT/IFFT. The new algorithm can correctly give transient lower bound and upper bounds of the performance variations of analog circuits accurately and reliably. Experimental results on several industry benchmark circuits demonstrate the effectiveness and efficiency of the proposed method against the Monte Carlo method. The new method can deliver about one order of magnitude speedup over the Monte Carlo method.

We organize the remaining parts of the paper as follows. Section II gives the overall flow of the proposed method and reviews the first two steps in the proposed method. Section III discusses in detail the newly proposed general-signal transient performance bound analysis algorithm. Experiments in Section IV shows the simulation results of several circuits under process variation and comparison results against the Monte

This research was supported in part by NSF grants under No. CCF-1116882, No. OISE-1130402, No. OISE-0929699, and in part by a UC MEXUS-CONACYT collaborative research grant (2011-2013).

978-1-4673-0772-7/12/$31.00 ©2012 IEEE

Carlo method. Finally, Section V concludes this paper.

II. The proposed algorithm — TIDBA

In this section, we first present the whole TIDBA algorithm flow, which is shown in Fig. 1. Then we explain each step in detail in the following sections. The new algorithm flow consists of three major steps as shown in the flow. The first step computes the variational transfer function from a linearized analog circuits by a graph-based symbolic analysis with affine arithamtic. The second step computes the performance bounds (magnitude and phase) of the transfer function via Kharitonov's funtions. The last steps converts frequency-domain performance bounds into the time-domain performance bounds by impulse signal based time-domain bound analysis and FFT/IFFT, which will be the focus of this paper.

Algorithm 1 The algorithm flow of the new time-domain performance bound analysis method — TIDBA

Input: circuit netlist with variable parameters; stimulus signal of the circuit.

Output: lower and upper bounds of the output signal in time-domain.

1: Compute the variational transfer function by graph-based symbolic method and affine arithmetic method.
2: Compute the performance bounds of the variational transfer function by Kharitonov's theorem.
3: Compute the time-domain performance bounds by a new general-signal transient bound analysis using FFT/IFFT.

In the sequel, we first review the first two steps that compute the performance bounds of analog circuits in frequency domain, which is based on a recently proposed method [2].

A. Computing of varitional transfer functions

In this paper, we still model the variations of component values as intervals measured from tested chip and manufacture processes. Then determinant decision diagram (DDD) based symbolic analysis approach [15] is applied to obtain the symbolic expression of transfer functions from the linearized analog circuits. The coefficients of the transfer functions can be represented by the so-called multi-rooted DDD graphs exactly [16]. Once a DDD has been constructed, the numerical values of the determinant can be computed by performing the depth-first type search of the graph and performing simple addition and multiplication at each node. After this, instead of performing simple arithemtic operations, affine arithmetic operations [1] are performed at each DDD node to compute the interval values of each root. Consequently, these root values, represented by affine intervals, will essentialy be the interval coefficients of the transfer function.

Suppose that each circuit parameter $\hat{x}$ becomes an affine interval $\hat{x} = x_0 + \sum_{i=1}^{n} x_i \varepsilon_i$ due to process variations. The resulting transfer functions will take the following s-expanded rational form:

$$H(s,\hat{x}) = \frac{N(s,\hat{x})}{D(s,\hat{x})} = \frac{\sum_{i=0}^{m} \hat{a}_i(\hat{x}) s^i}{\sum_{j=0}^{n} \hat{b}_j(\hat{x}) s^j} \tag{1}$$

where coefficients $\hat{a}_i(\hat{x})$ and $\hat{b}_j(\hat{x})$ are all affine intervals.

B. Computing of performance responses of the variational transfer functions

Once we have the variational transfer function represented in (1), we can obtain its frequency-domain response bounds (in terms of magnitude and phase) using Kharitonov's functions [3], which can give the approved bounds of responses in frequency domain. Kharitonov's functions [3] were proposed originally for checking the stability issues of a polynomial with coefficient uncertainties (due to perturbations). Later, Levkovich etc. [7] showed that Kharitonov's theorem can be used to calculate the magnitude and phase envelops of a family of interval rational transfer functions of continuous-time systems in frequency domain.

After this step, the bounds of magnitude and phase (angle) of the transfer function $H(j\omega) = H(\omega)e^{j\theta(\omega)}$ become available, i.e.,

$$H_l(\omega) \le H(\omega) \le H_u(\omega) \tag{2}$$

$$\theta_l(\omega) \le \theta(\omega) \le \theta_u(\omega), \tag{3}$$

where $H_l(\omega)$, $H_u(\omega)$ are the lower and upper bounds of the magnitude and $\theta_l(\omega)$ and $\theta_u(\omega)$ are the lower and upper bounds of phase.

III. Computing of the Performance Bound in Time Domain

In this section, we present the new transient performance bound analysis method, which converts the frequency domain bounds to time-domain bounds for general signals. Our approach was inspired by [12], which determines time-domain performance bounds of an uncertain system for impulse or step signal input signals. However, this method does not give general-signal transient performance bounds, which are required by our analog/mixed-signal circuit analysis. In the sequel, we first briefly review the work in [12] before introducing our new approach.

A. Transient bound analysis driven by impulse signal

For a purely real $x(t)$ in time domain, its Fourier transform $X(j\omega) = X(\omega) \cdot e^{j\phi(\omega)}$ in frequency domain holds the property of conjugate symmetry, i.e.,

$$X(-j\omega) = X(j\omega)^*. \tag{4}$$

It can be equivalently expressed by the even property of magnitude and the odd property of phase: $X(-\omega) = X(\omega)$, and $\phi(-\omega) = -\phi(\omega)$. It is not difficult to show that the transfer function of a physically realizable system also holds the conjugate symmetry property [6].

Since the spectrum of an impulse signal $\delta(t)$ is $X(j\omega) = 1$ everywhere, the spectrum of the system's output signal is $Y(j\omega) = X(j\omega)H(j\omega) = H(j\omega)$, and hence the impulse response of the system at time domain is simply the inverse Fourier transform of $H(j\omega)$,

$$\begin{aligned} y(t) &= \frac{1}{2\pi}\int_{-\infty}^{\infty} H(j\omega)e^{j\omega t}\,\mathrm{d}\omega \\ &= \frac{1}{2\pi}\int_{-\infty}^{\infty} H(\omega)e^{j(\omega t+\theta(\omega))}\,\mathrm{d}\omega, \quad t>0. \end{aligned} \tag{5}$$

Employing the even and odd properties of $H(j\omega)$, (5) can be equivalently integrated from $\omega = 0$ to ∞,

$$y(t) = \frac{1}{\pi}\int_0^\infty H(\omega)\mathrm{Re}(e^{j(\omega t+\theta(\omega))})\,\mathrm{d}\omega$$
$$= \frac{1}{\pi}\int_0^\infty H(\omega)\cos(\omega t+\theta(\omega))\,\mathrm{d}\omega, \quad t>0. \quad (6)$$

A modification of this integral to discrete sum on sampled frequency points allows one to calculate the approximate result of $y(t)$ at each time point as

$$y(t) = \frac{1}{\pi}\sum_{n=0}^{N-1}\underbrace{H(\omega_n)\cos(\omega_n t+\theta(\omega_n))}_{I(\omega_n)}\Delta\omega_n, \quad t>0. \quad (7)$$

In the presence of process variation, the transfer function will be given in the bounded form in (2) and (3). Therefore, to compute the lower and upper transient bounds $y_l(t)$ and $y_u(t)$ for each time point t, the integrand body $I(\omega_n)$ in (7) is calculated using the following rules.

First, find the minimum and maximum values of $\cos(\omega_n t+\theta(\omega_n))$, where the phase angle $\theta(\omega_n)$ can vary in the interval $[\theta_l(\omega_n), \theta_u(\omega_n)]$. Let $C_{\min}(\omega_n)$ and $C_{\max}(\omega_n)$ denote the two extreme values of the cosine function. Then, for $y_l(t)$, all $I(\omega_n)$ shall be calculated as

$$I(\omega_n) = \begin{cases} H_u(\omega_n)C_{\min}(\omega_n), & C_{\min}(\omega_n)\le 0 \\ H_l(\omega_n)C_{\min}(\omega_n), & C_{\min}(\omega_n)>0, \end{cases} \quad (8)$$

and, for $y_u(t)$, the situation is simply reversed,

$$I(\omega_n) = \begin{cases} H_l(\omega_n)C_{\max}(\omega_n), & C_{\max}(\omega_n)\le 0 \\ H_u(\omega_n)C_{\max}(\omega_n), & C_{\max}(\omega_n)>0. \end{cases} \quad (9)$$

B. Proposed general-signal transient bound analysis method

For a general time domain signal $x(t)$ in real application, its frequency-domain transform $X(j\omega)$ can be calculated by fast Fourier transform, FFT. This requires sampling points of the signal on a set of discretized time points. For example, with a uniform sampling period $T_s = 1/F_s$, $x(t)$ is sampled and stored as $x(0)$, $x(T_s)$, $x(2T_s)$,..., $x(NT_s)$. For the sake of simplicity, we will omit the term T_s and denote the time point indices by subscripts in the following descriptions. Thus the notation x_n will stand for the sampled value of signal $x(t)$ at time $t = nT_s$.

To achieve accurate results from FFT and IFFT, Nyquist sampling theorem requires the sampling frequency $F_s = 1/T_s$ to be at least twice of the bandwidth of signal [10]. Meanwhile, the total sampling duration $T_0 = T_s N$ determines the resolution of the FFT spectrum, i.e., the sampling interval of frequency domain is $F_0 = 1/T_0$. The longer T_0 is, the higher resolution we can get, and thus the more sampling points are needed.

Given N sampling points, the FFT transform pair is

$$X_k = \sum_{n=0}^{N-1} x_n e^{-j\frac{2\pi}{N}nk}, \quad k=0,1,\ldots,N-1, \text{ and} \quad (10)$$

$$x_n = \frac{1}{N}\sum_{k=0}^{N-1} X_k e^{j\frac{2\pi}{N}nk}, \quad n=0,1,\ldots,N-1. \quad (11)$$

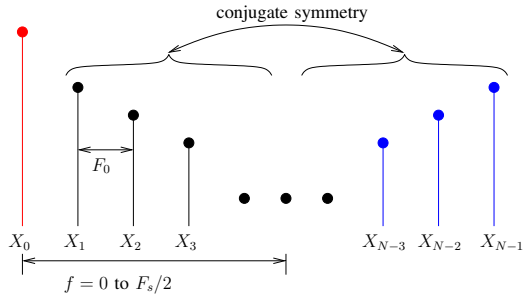

Fig. 1. Conjugate symmetry between left half and right half of the FFT series X_k, $k = 0,\ldots,N-1$.

In circuit analysis applications, because the input data x_n are purely real, the symmetry property mentioned previously still holds, though in a different form, $X_{N-k} = X_k^*$. This means that the right half in X_k is a conjugate swap of its left half without X_0, which is the zero-frequency component of the spectrum. The points in the left half, i.e., X_k for $k = 0,\ldots,N/2$, are the spectral points of frequencies $f = kF_0$. Fig. 1 illustrates the FFT series and its conjugate symmetry.

Based on this property of a real signal's spectrum, the inverse discrete Fourier transform can be calculated with the spectrum's left half. Consequently, the equivalent form of (11) becomes

$$x_n = \frac{1}{N}\left[X_0 + 2\sum_{k=1}^{N/2}\mathrm{Re}(X_k e^{j\frac{2\pi}{N}nk})\right], \quad n=0,1,\ldots,N-1. \quad (12)$$

We remark that throughout this paper the expression using only left half is mainly for the convenience of mathematical analysis. In practice, full spectrum is constructed before the final converting to time domain, and thus IFFT is ready to be applied for its efficiency.

Now it is the time to derive the time response bounds from the FFT series of signal $x(t)$ given the frequency bounds of the system $H(j\omega)$. First we consider the system without variation. After the FFT of x_n as represented in (10), its spectrum $X_k = |X_k|e^{j\phi_k}$ is multiplied with $H_k = H(j\omega_k)$, $\omega_k = 2\pi kF_0$, to obtain the spectrum of output signal. Then, we make a domain translation from frequency domain to time domain, which is similar to (12). In this way, the output signal y_n is obtained for the nominal designed system.

$$y_n = \frac{1}{N}\left[Y_0 + 2\sum_{k=1}^{N/2}\mathrm{Re}\left[Y_k e^{j\frac{2\pi}{N}nk}\right]\right]$$
$$= \frac{1}{N}\left[X_0H(0) + 2\sum_{k=1}^{N/2}\mathrm{Re}\left[H(\omega_k)e^{j\theta(\omega_k)}X_k e^{j\frac{2\pi}{N}nk}\right]\right]$$
$$= \frac{1}{N}\left[X_0H(0) + 2\sum_{k=1}^{N/2}|X_k|H(\omega_k)\mathrm{Re}\left[e^{j(\phi_k+\theta(\omega_k)+\frac{2\pi}{N}nk)}\right]\right] \quad (13)$$

Now we consider the process variaitons. In this case, the minimum and maximum values, similar to (8) and (9) for the

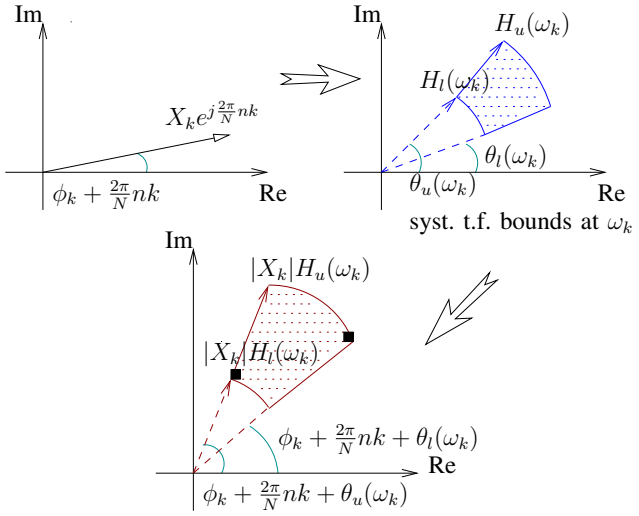

Fig. 2. The magnification and rotation of input spectrum by the transfer function bounds.

impulse signals, have to be derived in the bounded region of the system transfer function at every frequency point. Specifically, the selection and combinations of $H(\omega)$ and $\theta(\omega)$ will depend on the sign of the real part of the output spectrum, i.e., $\mathrm{Re}\{e^{j(\phi_k+\theta(\omega_k)+\frac{2\pi}{N}nk)}\}$. Detailed analysis shows that there are many combinations of exetreme values of $H(\omega)$ and $\theta(\omega)$ depending on the locations of $\phi_k + \theta(\omega_k) + \frac{2\pi}{N}nk$ in the complex plane, which are summerized in Table I. Let's walk through one example illustrated in Fig. 2, where all possible values of $\theta(\omega_k)$ make the phase $\phi_k + \theta(\omega_k) + \frac{2\pi}{N}nk$ fall in the first quadrant, and thus their real parts are all positive. Therefore, the selection of $H_l(\omega_k)$ and $\theta_u(\omega_k)$ will lead to the minimum of output value, while $H_u(\omega_k)$ and $\theta_l(\omega_k)$ lead to the maximum one. In Fig. 2, these two combinations are marked by black dots.

We remark that the range of allowed phase values $[\theta_l(\omega_k), \theta_u(\omega_k)]$ affects the rules for bound determination, as shown in Table I. In this paper, we restrict the maximum phase range to be less than 90 degrees, i.e., $\theta_u(\omega_k) - \theta_l(\omega_k) < \pi/2$ rads. There are two reasons for this restriction: 1) The restriction of 90 degrees accommodates most circuit transfer function's variation very well. 2) If much larger phase variation is detected at the frequency domain, the variation will likely casue faults in the circuit . We stress that there is no difficulty to generate new bound determination rules to handle phase range larger than 90 degrees.

With this assumption, the rules for time domain bound determination is summarized in Table I. For brevity, let $\Theta_l(\omega_k) = \phi_k + \theta_l(\omega_k) + \frac{2\pi}{N}nk$, and $\Theta_u(\omega_k) = \phi_k + \theta_u(\omega_k) + \frac{2\pi}{N}nk$. If the range of Θ is not covered by the enumerated regions, a phase shift of 2π can be applied to relocate its value within the listed ranges. In addition, the "either $\Theta_l(\omega_k)$ or $\Theta_u(\omega_k)$" in the first row and the fifth row in the table means one of them will be selected: in the first row, the lower bound will happen at the one of them which makes $\cos(\Theta)$ smaller; and in the fifth row, the upper bound will take place at the phase angle making $\cos(\Theta)$ larger.

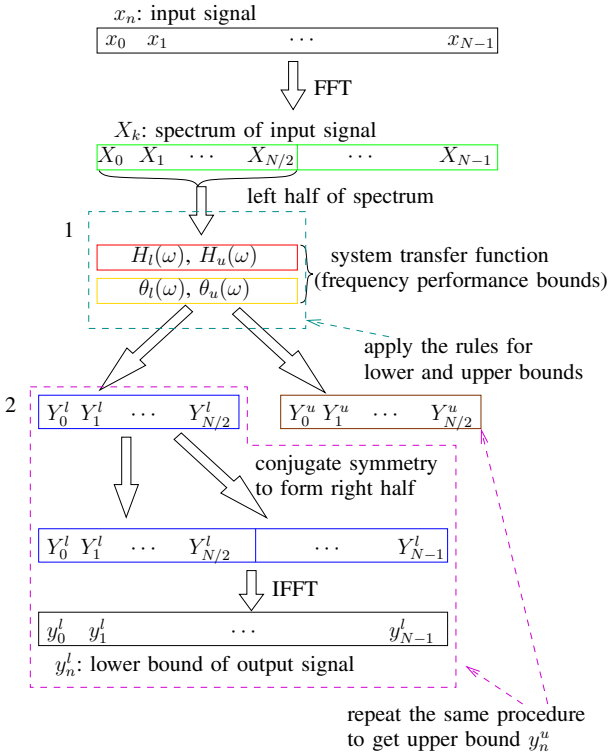

Fig. 3. The proposed general-signal transient bound determination method

Fig. 3 shows the implementation flow of the proposed general-signal transient bound determination method. It starts from a time domain sampling of input signal $x(t)$ and given system transfer function bounds in frequency domain. The FFT operation transforms input signal to its spectrum and then the proposed rules in Table I are applied to determine the magnitude and phase combinations for lower and upper time domain bounds at every frequency point in the left half of the spectrum. This process is marked by the dashed line box, labeled "1" in Fig. 3. Next, frequency domain results, i.e., $Y_0, Y_1, \ldots, Y_{N/2}$, either lower ones or upper ones, are used to construct a full N-length series based on conjugate symmetry property. Last, IFFT is used to calculate the final result of time domain bounds. This procedure is also marked by dashed line box, labeled "2" in the figure.

IV. Numerical Experiments

The proposed TIDBA method has been implemented using C into a software tool that can read in general SPICE circuit netlists and variational parameters. With process variation, TIDBA then generates the magnitude and phase bounds of the transfer function and then generates the transient performance bounds.

The whole experiments were run on a Linux server with a 3 GHz Intel Xeon quad-core CPU and 16 GBytes memory. The proposed bound analysis were evaluated from two sample circuits, a CMOS low-pass filter, shown in Fig. 4, and a CMOS cascode opamp. In both cases, the small signal model is used to load the MOSFET transistors.

Fig. 5 shows the calculated frequency response bounds of

TABLE I
RULES FOR TIME DOMAIN BOUND DETERMINATION.

range of phase		quadrants	sign of real part	magnitude and phase combinations for	
$\Theta_l(\omega_k)$	$\Theta_u(\omega_k)$			lower bound	upper bound
$(-\pi/2, 0)$	$(0, \pi/2)$	IV, I	$+$	$H_l(\omega_k)$, either $\Theta_l(\omega_k)$ or $\Theta_u(\omega_k)$	$H_u(\omega_k)$, $\Theta(\omega_k) = 0$
$(0, \pi/2)$	$(0, \pi/2)$	I	$+$	$H_l(\omega_k)$, $\Theta_u(\omega_k)$	$H_u(\omega_k)$, $\Theta_l(\omega_k)$
$(0, \pi/2)$	$(\pi/2, \pi)$	I	$+, -$	$H_u(\omega_k)$, $\Theta_u(\omega_k)$	$H_u(\omega_k)$, $\Theta_l(\omega_k)$
$(\pi/2, \pi)$	$(\pi/2, \pi)$	II	$-$	$H_u(\omega_k)$, $\Theta_u(\omega_k)$	$H_l(\omega_k)$, $\Theta_l(\omega_k)$
$(\pi/2, \pi)$	$(\pi, 3\pi/2)$	II, III	$-$	$H_u(\omega_k)$, $\Theta(\omega_k) = \pi$	$H_l(\omega_k)$, either $\Theta_l(\omega_k)$ or $\Theta_u(\omega_k)$
$(\pi, 3\pi/2)$	$(\pi, 3\pi/2)$	III	$-$	$H_u(\omega_k)$, $\Theta_l(\omega_k)$	$H_l(\omega_k)$, $\Theta_u(\omega_k)$
$(\pi, 3\pi/2)$	$(3\pi/2, 2\pi)$	III, IV	$+, -$	$H_u(\omega_k)$, $\Theta_l(\omega_k)$	$H_u(\omega_k)$, $\Theta_u(\omega_k)$
$(3\pi/2, 2\pi)$	$(3\pi/2, 2\pi)$	IV	$+$	$H_l(\omega_k)$, $\Theta_l(\omega_k)$	$H_u(\omega_k)$, $\Theta_u(\omega_k)$

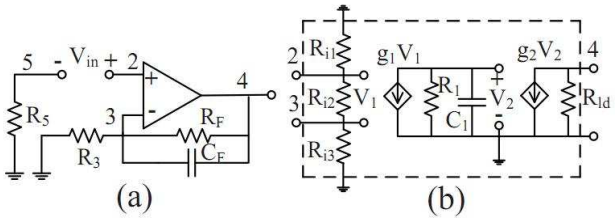

Fig. 4. (a) Schematic of a low-pass filter. (b) Linear model of the opamp.

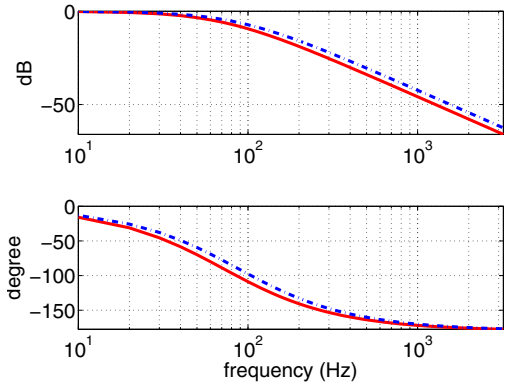

Fig. 5. Frequency response bounds of a CMOS low-pass filter.

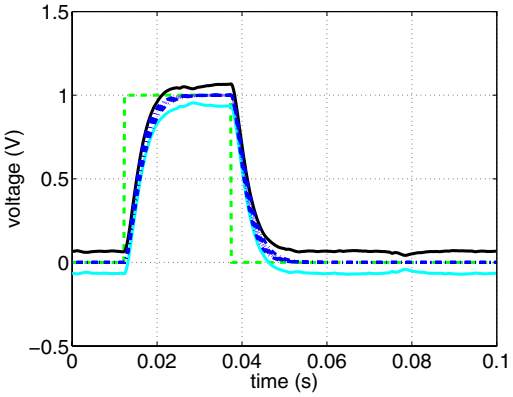

(a) The whole plot

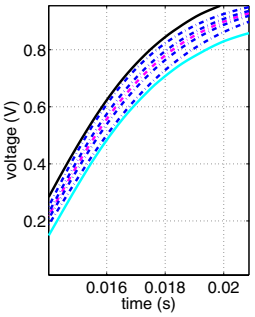

(b) Detail of up ramp

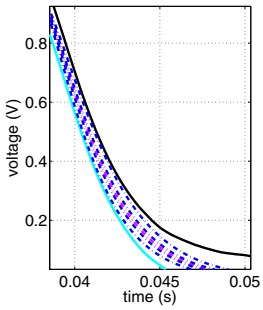

(c) Detail of down ramp

Fig. 6. Time domain response of the low-pass filter with pulse wave input. The two solid curves are the lower and upper bounds, while the region marked by dot-dashed lines are possible output waveforms from Monte Carlo simulation affected by variations.

a CMOS low-pass filter by the aforementioned affine DDD method. We have simulated this filter with a pulse waveform as input, and the resulted output waveforms are plotted as dot-dashed curves in Fig. 6. Due to the process variation of the filter, it can be observed that the output waveforms are deviated from its nominal benchmark. Detailed plots of the up ramp and down ramp are shown in the Fig. 6(b) and Fig. 6(c). The time domain performance bounds, computed by TIDBA, are plotted as solid curves. An input signal of several sinusoidal waves are also used to test this filter. Its possible minimum and maximum values in the time domain and the TIDBA bounds are plotted in Fig. 7. A bunch of pulse responses at the output node of cascode opamp are plotted in Fig. 8, and the bounds generated from TIDBA are overlaid onto the figure as solid curves.

We notice that the bounds given by TIDBA do not converge to the steady state of the response, for example, after 0.06 second in Fig. 6(a), which should be zero. This is due to the loss of dependence between magnitude and phase when we apply the frequency response bounds (2) and (3). However, TIDBA still accurately encloses the fast changing transient behavior of the waveform responses as shown in the figures.

Table II enumerates the experiment parameters and running time comparisons. In the low-pass filter netlist, three variational parameters are introduced, including resistor, capacitor, and controlled source inside the opamp as local variations, and four other parameters are modeled as global variations. For the cascode opamp, it is modeled in a similary way. We make these variational parameters Gaussian random and run a 10000 times Monte Carlo simulation in HSPICE. A total number of 6400

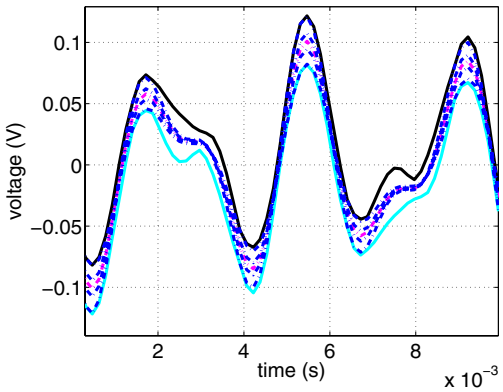

Fig. 7. Time domain response of the low-pass filter with sinusoidal wave input. The two solid curves are the lower and upper bounds, while the region marked by dot-dashed lines are possible output waveforms from Monte Carlo simulation affected by variations.

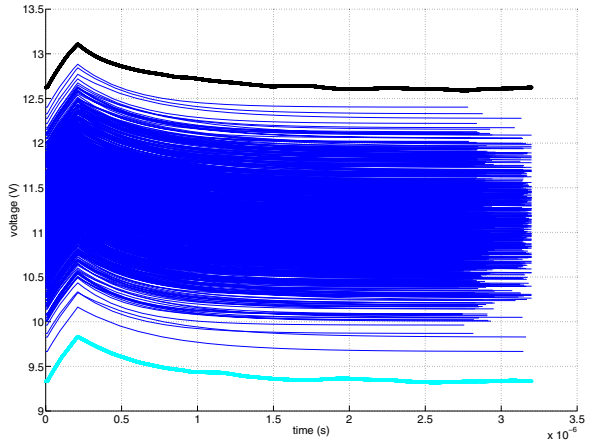

Fig. 8. Time domain response of CMOS cascode opamp with pulse input. The two thicker curves are the lower and upper bounds from TIDBA, while the thiner lines are output waveforms from Monte Carlo simulation affected by variations.

time domain samplings of input stimulus are fed into FFT. The running time measurements of the Monte Carlo and our proposed non-Monte Carolo method are also listed in the table. For these four experiment setup, the maximum speedup of TIDBA over Monte Carlo simulation can be 38×.

V. Conclusion

In this paper, we have proposed a new transient performance bound analysis method for analog circuits with process variations. The new method, named *TIDBA*, employs several techniques. It first computes the performance bound in frequency domain using graph-based symbolic analysis, affine interval and Kharitonov's functions. Then it converts the frequency domain response bound to the time domain bound by a new general-signal transient bound analysis method using FFT/IFFT. Experimental results from two industry benchmark circuits have shown that TIDBA gives the correct bounds for the Monte Carlo analysis while it delivers one order of magnitude speedup over the Monte Carlo method.

TABLE II
Performance comparison of TIDBA againt the Monto Carlo method

Circuit name	# Var. param	Variation local	Variation global	CPU time MC (10^4)	CPU time TIDBA	speed up
low pass	7	5%	10%	459.7 s	11.9 s	38×
		10%	10%	470.1 s	12.5 s	37×
cascode	30	5%	10%	362.9 s	13.6 s	27×
		10%	10%	345.7 s	11.2 s	31×

References

[1] L. H. de Figueiredo and J. Stolfi, "Self-validated numerical methods and applications," in *Brazilian Mathematics Colloquium monographs*, IMPA/CNPq, Rio de Janeiro, Brazil, 1997.

[2] Z. Hao, R. Shen, S. X.-D. Tan, and G. Shi, "Performance bound analysis of analog circuits considering process variations," in *Proc. Design Automation Conf. (DAC)*, July 2011, pp. 310–315.

[3] V. L. Kharitonov, "Asymptotic stability of an equilibrium position of a family of systems of linear differential equations," *Differential. Uravnen.*, vol. 14, pp. 2086 –2088, 1978.

[4] J. Kim, K. Jones, and M. Horowitz, "Fast, non-monte-carlo estimation of transient performance variation due to device mismatch," in *Proc. IEEE/ACM Design Automation Conference (DAC)*, 2007.

[5] L. Kolev, V. Mladenov, and S. Vladov, "Interval mathematics algorithms for tolerance analysis," *IEEE Trans. on Circuits and Systems*, vol. 35, no. 8, pp. 967 –975, Aug. 1988.

[6] B. P. Lathi, *Modern Digital and Analog Communication Systems*, 3rd ed. Oxford University Press, 1998.

[7] A. Levkovich, E. Zeheb, and N. Cohen, "Frequency response envelopes of a family of uncertain continuous-time systems," *IEEE Trans. on Circuits and Systems I: Fundamental Theory and Applications*, vol. 42, no. 3, pp. 156 –165, Mar. 1995.

[8] H. Masuda, S. Ohkawa, A. Kurokawa, and M. Aoki, "Challenge: Variability characterization and modeling for 65- to 90-nm processes," in *Proc. IEEE Custom Integrated Circuits Conf.*, 2005.

[9] S. Nassif, "Model to hardware correlation for nm-scale technologies," in *Proc. IEEE International Workshop on Behavioral Modeling and Simulation (BMAS)*, Sept 2007, keynote speech.

[10] A. V. Oppenheim and R. W. Schafer, *Discrete-Time Signal Processing*. Prentice Hall, 1999.

[11] M. Pelgrom, A. Duinmaijer, and A. Welbers, "Matching properties of mos transistors," *IEEE J. of Solid State Circuits*, pp. 1433–1439, 1989.

[12] C. Pritchard and B. Wigdorowitz, "Improved method of determining time-domain transient performance bounds from frequency response uncertainty regions," *International Journal of Control*, vol. 66, no. 2, pp. 311 – 327, 1997.

[13] L. Qian, D. Zhou, S. Wang, and X. Zeng, "Worst case analysis of linear analog circuit performance based on kharitonov's rectangle," in *Proc. IEEE Int. Conf. on Solid-State and Integrated Circuit Technology (ICSICT)*, Nov. 2010.

[14] R. Rutenbar, "Next-generation design and EDA challenges," in *Proc. Asia South Pacific Design Automation Conf. (ASPDAC)*, January 2007, keynote speech.

[15] C.-J. Shi and X.-D. Tan, "Canonical symbolic analysis of large analog circuits with determinant decision diagrams," *IEEE Trans. on Computer-Aided Design of Integrated Circuits and Systems*, vol. 19, no. 1, pp. 1–18, Jan. 2000.

[16] ——, "Compact representation and efficient generation of s-expanded symbolic network functions for computer-aided analog circuit design," *IEEE Trans. on Computer-Aided Design of Integrated Circuits and Systems*, vol. 20, no. 7, pp. 813–827, April 2001.

[17] C.-J. R. Shi and M. W. Tian, "Simulation and sensitivity of linear analog circuits under parameter variations by robust interval analysis," *ACM Trans. Des. Autom. Electron. Syst.*, vol. 4, pp. 280–312, July 1999.

[18] R. Spence and R. Soin, *Tolerance Design of Electronic Circuits*. Addison-Wesley, Reading, MA., 1988.

[19] W. Tian, X.-T. Ling, and R.-W. Liu, "Novel methods for circuit worst-case tolerance analysis," *IEEE Trans. on Circuits and Systems I: Fundamental Theory and Applications*, vol. 43, no. 4, pp. 272 –278, Apr. 1996.

[20] J. Vlach and K. Singhal, *Computer Methods for Circuit Analysis and Design*. New York, NY: Van Nostrand Reinhold, 1995.